HHS Public Access

Author manuscript

Nat Neurosci. Author manuscript; available in PMC 2015 June 01.

Published in final edited form as:

Nat Neurosci. 2014 December ; 17(12): 1673–1681. doi:10.1038/nn.3858.

GLIAL ANKYRINS FACILITATE PARANODAL AXOGLIAL JUNCTION ASSEMBLY

Kae-Jiun Chang[1], **Daniel R. Zollinger**[2], **Keiichiro Susuki**[2], **Diane L. Sherman**[3], **Michael A. Makara**[4], **Peter J. Brophy**[3], **Edward C. Cooper**[2,5], **Vann Bennett**[6], **Peter J. Mohler**[4], and **Matthew N. Rasband**[1,2]

[1]Program in Developmental Biology, Baylor College of Medicine, Houston, TX 77030, USA

[2]Department of Neuroscience, Baylor College of Medicine, Houston, TX 77030, USA

[3]Centre for Neuroregeneration, University of Edinburgh, Edinburgh, United Kingdom EH16 4SB

[4]Departments of Physiology and Cell Biology, Medicine, and the Dorothy M. Davis Heart and Lung Research Institute, The Ohio State University, Columbus, OH 43210, USA

[5]Department of Neurology, Baylor College of Medicine, Houston, TX 77030, USA

[6]Department of Cell Biology, Duke University, Durham, NC 27710, USA

Abstract

Neuron-glia interactions establish functional membrane domains along myelinated axons. These include nodes of Ranvier, paranodal axoglial junctions, and juxtaparanodes. Paranodal junctions are the largest vertebrate junctional adhesion complex, are essential for rapid saltatory conduction, and contribute to assembly and maintenance of nodes. However, the molecular mechanisms underlying paranodal junction assembly are poorly understood. Ankyrins are cytoskeletal scaffolds traditionally associated with Na+ channel clustering in neurons and important for membrane domain establishment and maintenance in many cell types. Here, we show that ankyrinB, expressed by Schwann cells, and ankyrinG, expressed by oligodendrocytes, are highly enriched at the glial side of paranodal junctions where they interact with the essential glial junctional component neurofascin 155. Conditional knockout of ankyrins in oligodendrocytes disrupts paranodal junction assembly and delays nerve conduction during early development in mice. Thus, glial ankyrins function as major scaffolds that facilitate early and efficient paranodal junction assembly in the developing central nervous system.

*Correspondence should be addressed to: Dr. Matthew N. Rasband, Department of Neuroscience, Baylor College of Medicine, One Baylor Plaza, Houston, Texas 77030, Tel: 713-798-4494, Fax: 713-798-3946, rasband@bcm.edu.

AUTHOR CONTRIBUTIONS

M.N.R. and K.-J.C. conceived the project, designed the experiments and wrote the manuscript. D.R.Z. and K.S. performed the electrophysiology experiments and analyzed the data. D.R.Z. conducted the electron microscopy experiments. K.-J.C. performed all other experiments and analyzed the data. P.J.M. and M.A.M. designed and constructed the *Ank2*^{floxed} allele. D.L.S., P.J.B., E.C.C. and V.B. provided necessary reagents and mice.

Competing Financial Interests:

The authors declare no competing financial interests.

INTRODUCTION

Schwann cells in the peripheral nervous system (PNS) and oligodendrocytes in the central nervous system (CNS) wrap and insulate axons with myelin. They also actively cluster ion channels, cell adhesion molecules (CAMs), and cytoskeletal scaffolds to form distinct functional domains along axons[1,2]. For example, voltage-gated Na+ (Nav) channels are highly enriched at nodes of Ranvier, while interactions between glial and axonal CAMs flanking nodes form paranodal junctions. Together, myelin, clustered ion channels, and paranodal junctions make action potential propagation much faster and more efficient.

Paranodal junctions perform several important tasks including: (1) restricting nodal proteins to assemble and maintain nodes; (2) separating juxtaparanodal voltage-gated K+ (Kv1) channels from nodal Nav channels; and (3) separating the periaxonal and extracellular spaces to fulfill myelin's insulating role[3,4]. An interacting set of CAMs, including axonal contactin and Caspr (contactin-associated protein) and glial NF155 (the 155-kDa isoform of neurofascin), are highly enriched at paranodes and are vital constituents of the junctions[1,2]. Loss of any single paranodal CAM disrupts paranodal junctions, and causes delayed nerve conduction, tremor, and ataxia[4]. Despite their importance, the mechanisms regulating clustering and maintenance of paranodal CAMs remain unknown.

Ankyrins participate in formation and stabilization of membrane subdomains in many cell types[5,6]. In the nervous system, ankyrinG (AnkG) is expressed by neurons and enriched at the axon initial segment (AIS) and node, where AnkG clusters Nav channels[7–10]. AnkyrinB (AnkB) is found in unmyelinated axons and regulates AIS assembly by establishing an intra-axonal boundary limiting AnkG's incorporation into the distal axonal submembranous cytoskeleton[11,12]. When axons are myelinated, in addition to nodal AnkG, AnkB and AnkG are detected at paranodes in the PNS and CNS, respectively[13,14]. Given the important roles of ankyrins in axon domain organization, we investigated whether ankyrins contribute to the assembly and function of paranodes. Surprisingly, in contrast to previous reports, we found paranodal AnkB and AnkG are not axonal, but glial paranodal scaffolding proteins that interact with NF155. Furthermore, conditional knockout of ankyrins in oligodendrocytes disrupted paranodal junction formation and delayed nerve conduction during early CNS development. These results reveal a mechanism where glial paranodal ankyrins interact with NF155 to facilitate rapid paranodal junction assembly in the CNS.

RESULTS

Paranodal AnkB is in Schwann cells

The cytoskeletal scaffold AnkB is highly enriched at paranodal junctions in the PNS (Fig. 1a) and was reported to be in axons[13]. To determine if AnkB is important for paranodal junction assembly, we silenced AnkB expression in cultured dorsal root ganglion (DRG) neurons by using a highly efficient shRNA (short hairpin RNA) and GFP (green fluorescent protein)-expressing construct delivered by adenovirus[12]. AnkB protein expression was efficiently eliminated from GFP-labeled axons (Fig. 1b). However, after axons were myelinated by co-culturing with Schwann cells, most of the GFP-labeled axons still showed clear paranodal AnkB that accumulated at the edges of myelin sheaths (Fig. 1c). One

explanation for the remaining paranodal AnkB immunoreactivity is that a very small amount of residual AnkB may be sufficient to form paranodal clusters. Alternatively, paranodal AnkB may be in Schwann cells and unaffected by the shRNA in neurons. In support of the latter possibility, we found that: (1) for some myelinated axons paranodal AnkB was located outside the GFP-labeled axons (Fig. 1d), and (2) immunoblots comparing purified cultured Schwann cells with cultured hippocampal neurons showed low levels of AnkB in Schwann cells (Fig. 1e).

To clearly determine if paranodal AnkB is in axons or Schwann cells, we co-cultured *AnkB-null*[15] DRG neurons and wild-type Schwann cells, and then induced myelination. Consistent with the possibility that paranodal AnkB is in Schwann cells, in the absence of axonal AnkB, we still observed paranodal AnkB (Fig. 1f). Together, these results show that AnkB is a glial component of paranodal junctions.

AnkB is not required for PNS paranodal junction assembly

To study the role of paranodal AnkB *in vivo*, we removed AnkB specifically from myelinating glia by crossing *Ank2-floxed* mice with *Cnp-Cre* mice[16] (*AnkB-cKO* or *Cnp-Cre;Ank2*$^{f/f}$; Fig. 1g); conventional AnkB knockout mice on a C57BL/6 background die at postnatal day (P) 0 before paranodal junctions form (data not shown). In *AnkB-cKO* sciatic nerves, AnkB staining was eliminated from paranodes (Fig. 1h, i), consistent with the fact that paranodal AnkB is in Schwann cells and suggesting that neurons contribute no detectable AnkB to paranodal junctions. However, despite the strong enrichment of AnkB at paranodes in control mice (*Cnp-Cre;Ank2*$^{f/+}$ or *AnkB-cHet*), paranodal junctions, defined by Caspr, NF155, and contactin, were assembled properly in *AnkB-cKO* mice (P28–P42 shown in Figs. 1h, i and 2a, b). In addition to their septate-like axoglial junctions, paranodes also have autotypic tight, adherens, and gap junctions between adjacent cytoplasmic loops[2]. In the *AnkB-cKO* mice, paranodal tight junctions (Fig. 2c), adherens junctions, gap junctions (data not shown), and the distribution of other paranodal loop components (Fig. 2d–g) were all unaffected, indicating AnkB is not essential for the overall architecture of PNS paranodes.

Paranodal junctions act as diffusion barriers that separate juxtaparanodal proteins from nodal proteins. Although the axonal paranodal scaffolds 4.1B and βII spectrin are not required for junction formation, they are crucial for barrier function[17–19]. To determine if paranodal AnkB plays a similar role in regulating juxtaparanodal protein localization from the glial side, we analyzed the distribution of Kv1.2 and Caspr2 in *AnkB-cKO* mice. We found that AnkB played no essential role in regulating juxtaparanodal protein localization (Fig. 2h, i). Consistent with the normal localization of nodal, paranodal, and juxtaparanodal proteins, we also measured no significant delay in the conduction velocity of compound action potentials (CAPs) along the *AnkB-cKO* sciatic nerves compared to wild-type (*WT* or *Ank2*$^{f/f}$) nerves at P56 (*WT*: 20.89 ± 1.16 m/s (mean ± SEM; N = 5 nerves); *AnkB-cKO*: 19.08 ± 1.14 m/s (N = 6); unpaired two-tailed *t* test: $p = 0.297$).

We considered whether loss of AnkB could delay paranode formation, or result in eventual paranode degeneration and loss of polarized axon domains in aged mice. However, we found that paranodal junctions formed normally in P3 sciatic nerves (Fig. 2j), and one-year-

old *AnkB-cKO* mice had normal paranodes and juxtaparanodal clustering of Caspr2 (Fig. 2k). Finally, paranodal junctions have previously been implicated in switching of nodal Nav channel subtypes from Nav1.2 to Nav1.6 during development, since mice with disrupted paranodal junctions retain Nav1.2 at nodes[20,21]. However, nodes in *AnkB-cKO* mice had Nav1.6 but no Nav1.2 (Fig. 2l), indicating that AnkB is not involved in the signaling pathway that regulates Nav channel subtype expression. Together, these results demonstrate that AnkB is a glial paranodal protein, but surprisingly is not required for paranodal junction formation, function, or maintenance.

AnkG is clustered at the glial side of CNS paranodes

Immunostaining of the dorsal root entry zone showed that AnkG is enriched at nodes and CNS paranodes (Fig. 3a), while AnkB is found at PNS paranodes; we only occasionally observed AnkB at CNS paranodes (Fig. 3a)[13]. Although AnkG has been strongly implicated in Nav channel clustering at nodes[8,10], the role and cellular source of paranodal AnkG are unknown.

Since paranodal AnkB is made by Schwann cells in the PNS, and since AnkG transcripts are 5.7 times more enriched in oligodendrocytes compared to neurons and astrocytes[22], we wondered if paranodal AnkG is also found in myelinating oligodendrocytes where it could contribute to paranodal junction assembly. To test this possibility, we generated AnkG-deficient oligodendrocytes by crossing *Ank3-floxed* mice with *Cnp-Cre* mice (*AnkG-cKO* or *Cnp-Cre;Ank3*$^{f/f}$; Fig. 3b). Control mouse optic nerves showed both nodal and paranodal AnkG immunoreactivity (Fig. 3c, d). However, *AnkG-cKO* mice had only nodal AnkG (Fig. 3e), indicating that paranodal AnkG is found in oligodendrocytes. Thus, myelinating Schwann cells have paranodal AnkB, while myelinating oligodendrocytes have paranodal AnkG.

AnkG is required for rapid CNS paranodal junction assembly

To determine if paranodes require AnkG for normal function, we examined their assembly during myelination in *AnkG-cKO* mice. Prior to the formation of full nodes (defined here as nodal clusters of βIV spectrin flanked by Caspr-labeled paranodal junctions on both sides), three kinds of nodal intermediates can be observed: (1) paranodes only, (2) nodes alone without flanking paranodal junctions, and (3) heminodes with paranodal junctions only on one side[14,23] (Fig. 3h). We found in the optic nerves of P12 control mice that the majority of nodal βIV spectrin clusters are flanked by one or two Caspr-labeled paranodes (Fig. 3f, h). In sharp contrast, the majority of nodal βIV spectrin clusters in *AnkG-cKO* optic nerves lacked flanking paranodal Caspr (Fig. 3g, h). The defect in paranodal junction assembly was due to mislocalization of junctional CAMs since their protein levels were comparable between the control and cKO optic nerves (Fig. 3i). This defect was further reflected in a significant delay in the CAP conduction velocity in P17 *AnkG-cKO* optic nerves (Fig. 3j, k). Thus, oligodendroglial AnkG is required for normal paranodal junction assembly and function.

Although we found a severe defect in paranodal junction assembly in the *AnkG-cKO* at P12, many paranodal junctions were still observed (Fig. 3h). Since AnkG contributes to both

assembly and maintenance of the AIS[9], we speculated that these AnkG-independent paranodal junctions might degenerate in older *AnkG-cKO* mice. However, a detailed analysis of nodes and nodal intermediates in P12–P56 *AnkG-cKO* optic nerves revealed that the number of paranodal junctions actually approached *WT* levels by P56 (Fig. 4a). Furthermore, we measured no delay in the CAP conduction velocity along P56 *AnkG-cKO* optic nerves compared to *WT* mice (data not shown), and juxtaparanodal clustering of Kv1 channels was normal in P22 (Fig. 4b) and 1-year-old *AnkG-cKO* mice (Fig. 4c). Together, these results suggest paranodal junctions are assembled less efficiently in the absence of paranodal AnkG, but they eventually recover and do not require AnkG for their maintenance.

AnkB partially compensates for loss of CNS paranodal AnkG

The gradual recovery of paranodal junction formation suggests that other mechanisms or molecules may compensate for the loss of AnkG. To determine if other ankyrins compensate, we examined the expression of the two other vertebrate ankyrins: AnkR and AnkB. Although we observed no AnkR at paranodes (data not shown), we did find many more AnkB-enriched paranodes in the *AnkG-cKO* optic nerves (Fig. 4d, e), suggesting AnkB may substitute for AnkG and rescue paranodal junction assembly in *AnkG-cKO* mice. We did not observe any increase in the levels of AnkB proteins and transcripts (data not shown), suggesting the paranodal AnkB immunoreactivity represents a re-distribution of AnkB proteins. To test whether AnkB compensates for the loss of AnkG, we constructed *AnkB/AnkG* double cKO mice (*AnkB/G-cKO*) using *Cnp-Cre* to remove both AnkB and AnkG from oligodendrocytes. *AnkB-cKO* mice showed no defects in paranodal junctions in the CNS (Fig. 4a, f). In contrast, when compared to *AnkG-cKO* mice, *AnkB/G-cKO* mice showed more severe defects in paranodal junction assembly throughout development (Fig. 4a, i). Thus, AnkB can partially compensate for the loss of AnkG in oligodendrocytes. We also observed defective paranodal junction assembly in spinal cord and corpus callosum (Supplementary Fig. 1), suggesting glial AnkG and AnkB are universally required for junction formation during early CNS development. Nevertheless, paranodal junctions, including transverse bands, still gradually formed and were properly maintained in the *AnkB/G-cKO* mice (Figs. 4g, h, j, k and 5a), and the differences between the *AnkB/G-cKO*, *AnkG-cKO*, and *WT* mice became smaller with increasing age (Fig. 4a). In addition, we observed similar percentages of nodes that are $Nav1.6^+$ or $Nav1.2^+$ between P56 *WT* and *AnkB/G-cKO* optic nerves (data not shown), indicating paranodal ankyrins are not essential for developmental switching of Nav channel subtypes.

Since myelination is a prerequisite for formation of nodes and paranodal junctions, one explanation for the changes described here is that myelination is delayed in the absence of glial ankyrins, and defective paranodal junction formation is secondary to delayed myelination. However, βIV spectrin was still clustered at nodes of Ranvier in *AnkG-cKO* and *AnkB/G-cKO* mice (Figs. 3g and 4a, i). Furthermore, electron microscopy of P17 *WT* and *AnkB/G-cKO* optic nerves showed no difference in the number or percentage of myelinated axons (Fig. 5b–d). These results indicate that myelination and paranodal junction assembly proceeds in the absence of ankyrins, but proper paranode formation occurs at a much reduced rate.

AnkB and AnkG interact with NF155

To understand the molecular mechanism whereby AnkG and AnkB regulate rapid paranodal junction assembly, we sought to identify their paranodal membrane protein binding partner. One possibility is that paranodal ankyrins function in concert with NF155, since NF155 is essential for paranodal junctions, and ankyrins bind to neurofascin's (NFasc) cytoplasmic domain[24,25]. To test this possibility, we examined NF155 and AnkB localization in developing sciatic nerves. We found NF155 enriched in subregions of paranodes where AnkB was located (Fig. 6a, c), suggesting that during early development NF155 localization is more closely aligned with AnkB than with Caspr. Furthermore, when AnkB extended beyond Caspr, NF155 extended together with AnkB (Fig. 6b, d). Although paranodal NF155 was previously reported to be phosphorylated[26] (which should block its interaction with ankyrins[24,25]), immunoprecipitation of AnkB from sciatic nerves and AnkG from spinal cords, in the presence of phosphatase inhibitors, co-precipitated NF155 (Fig. 6e, f). Together, these results suggest that some paranodal NF155 is not phosphorylated and interacts with paranodal ankyrins *in vivo*.

We previously proposed that during myelination, the initial interaction between glial NF155 and axonal Caspr/contactin assembles a paranodal lipid microdomain that promotes recruitment and stabilization of additional NF155 and Caspr/contactin molecules[27]. To determine if ankyrins contribute to these early events, we asked if they are recruited by NF155 to paranodal junctions. In *Caspr*$^{-/-}$ mice, paranodal junctions do not form[28,29] and most paranodes have no detectable AnkB at adulthood[13]. However, at 58% of paranodes in P7 *Caspr*$^{-/-}$ sciatic nerves, low levels of colocalized AnkB and NF155 could still be detected (Fig. 6g–i). A similar phenomenon of paranodal, colocalized AnkG and NF155 was also seen at 60% of paranodes in P7 *Caspr*$^{-/-}$ spinal cords (Fig. 6j–l). These observations suggest targeting of AnkB and AnkG to paranodes does not require intact paranodal junctions, and argue against the idea that ankyrins are passively recruited by NF155/Caspr/contactin junctional complexes. In addition, we analyzed sciatic nerve paranodal junctions from P5 *Nfasc*$^{-/-}$ mice transgenically rescued using NF155 that lacks its intracellular ankyrin-binding motif (NF155ΔIC)[30]. At 56% of paranodes identified by MAG enrichment, residual paranodal AnkB could be clearly observed (Fig. 6m–o). Similarly, residual paranodal AnkG was observed at 44% of paranodes in the P12 *Cnp-Cre;Nfasc*$^{f/f}$ spinal cord (Fig. 6p–r). These observations suggest that ankyrins can be targeted to paranodes independently of NF155.

Myelinating glia express 220-kDa AnkB from multiple promoters

Our discovery that glial ankyrins facilitate paranodal junction assembly, while axonal ankyrins participate in node and AIS assembly, is strikingly similar to the various contributions of alternatively spliced forms of NFasc: NF155 is expressed by myelinating glia and found at paranodes, while NF186 is expressed by neurons and found at nodes and the AIS. Similarly, previous studies have reported a variety of different ankyrin splice variants in the nervous system. For example, neurons express both 270- and 480-kDa AnkG isoforms at the AIS and nodes[7], and 440-kDa AnkB is expressed in unmyelinated axons[11,31]. To determine if distinct splice variants of AnkB and AnkG are utilized by glia at paranodal junctions or by axons, and how these different cell types regulate expression of

AnkB and AnkG, we designed isoform-specific primers and performed reverse transcription-quantitative polymerase chain reaction (RT-qPCR) analysis on P31 sciatic nerves and spinal cords. Alternative splicing of the 6.2-kb giant exon of *Ank2* (exon 41) can produce two AnkB isoforms: a 220-kDa AnkB produced by exclusion of exon 41, and a 440-kDa giant AnkB by inclusion of exon 41[5] (Fig. 7e and Supplementary Table 1). Exon 24 is removed by our conditional knockout strategy (Fig. 1g), and we detected a graded reduction in the exon 24-containing transcripts in the *AnkB-cHet* and *AnkB-cKO* sciatic nerves and spinal cords (Fig. 7a, d). Similarly, we observed a graded decrease in the levels of transcripts without exon 41 (220) but no significant decrease in the transcripts with exon 41 (440) (Fig. 7a, d). Consistently, Western blotting of sciatic nerve and spinal cord homogenates showed a dramatic reduction of 220-kDa AnkB in *AnkB-cKO* mice (Fig. 7b, c). These results suggest Schwann cells and oligodendrocytes express 220-kDa AnkB.

According to one previous study[32] and the current Ensembl database, there are five alternative promoters available to express AnkB. We designated the first exons driven by these promoters as exon 1″, exon 1′ (exon 0 in [32]), exon 1, exon ‘1 and exon 1s from upstream to downstream (Fig. 7e and Supplementary Table 1). To determine which first exon of AnkB is used by myelinating glia, we performed RT-qPCR to measure transcript levels; in our analysis we excluded exon 1s because our conditional knockout strategy only mildly affected exon 1s containing transcripts and antibodies specifically against AnkB’s spectrin-binding and C-terminal tail domains did not label paranodes in *AnkB-cKO* mice (data not shown). We found that myelinating glia in sciatic nerves and spinal cords use multiple promoters: Schwann cells mainly express exons 1- and ‘1-containing transcripts, while oligodendrocytes mainly express exons 1′- and ‘1-containing transcripts of AnkB (Fig. 7a, d).

Oligodendrocytes express 190/270-kDa AnkG from exon 1b

AnkG undergoes extensive alternative splicing[5]. Its splice variants include 480-, 270-, and 190-kDa isoforms depending on whether and how the giant exon (exon 41) is incorporated (Fig. 8f). To reveal isoforms expressed by oligodendrocytes, we performed RT-qPCR analysis on P31 spinal cords. Since exon 23 is removed by our conditional knockout strategy (Fig. 3b), we observed a graded decrease in exon 23-containing transcripts in the *AnkG-cHet* and *AnkG-cKO* mice (Fig. 8a). Among all the AnkG isoforms analyzed, the 190-kDa isoform-encoding transcripts showed the largest decrease, suggesting the majority of the 190-kDa isoform transcripts in P31 spinal cords are expressed by oligodendrocytes. Although the AIS and nodal 480-kDa isoform remained unchanged in the *AnkG-cHet* and *AnkG-cKO* mice, surprisingly the 270-kDa isoform also exhibited a graded decrease similar to that detected in exon 23, suggesting it is expressed by both neurons and oligodendrocytes. Therefore, we examined the localization of the 270-kDa isoform using antibodies specific for 480/270-kDa AnkG[7]. Consistent with our RT-qPCR results, the anti-480/270-kDa AnkG antibody stained both nodes and paranodes in *WT* mice (Fig. 8c), but failed to stain paranodes in *AnkG-cKO* mice. Immunoblots of spinal cord homogenates also showed decreases in the 190- and 270-kDa isoforms in the *AnkG-cKO* mice (Fig. 8b). Thus, oligodendrocytes express both 190- and 270-kDa AnkG.

Five alternative first exons have been identified for AnkG: 1a, 1b, 1e, 1f and 1s[33,34] (Supplementary Table 2). Because exon 1s is located between exons 25 and 26, exon 1s-containing AnkG should not be affected by our conditional knockout strategy (Figs. 8f and 3b). However, since our strategy eliminated paranodal AnkG, exon 1s-containing AnkG cannot be utilized by oligodendrocytes at paranodal junctions. To identify the AnkG promoter used by oligodendrocytes, we first stained spinal cord sections with antibodies against unique peptide sequences encoded by exons 1b and 1e[33]. We found that nodal AnkG includes exons 1b- and 1e-containing AnkG proteins, whereas oligodendrocytes only have exon 1b-containing AnkG at paranodes (Fig. 8d). To determine if exon 1a or 1f is also used by oligodendrocytes, we analyzed paranodal AnkG in the conventional KO of *Ank3* exon 1b, which is considered to be a cerebellum-specific KO[33]. Interestingly, paranodal AnkG was absent from *Ank3 exon 1b*$^{-/-}$ (Fig. 8e), indicating exon 1b is the main exon 1 utilized by oligodendrocytes and that this KO also affects oligodendrocytes. Consistent with these results, exon 1b-containing transcripts also showed a graded reduction in *AnkG-cHet* and *AnkG-cKO* mice (Fig. 8a). Thus, oligodendrocytes express 190-kDa and 270-kDa AnkG mainly from the promoter at exon 1b.

The alternative splicing of glial ankyrins compared to neuronal ankyrins reveals another level of complexity in neuron-glia interactions that parallels the situation for NFasc: neurons express NF186 and 480/270-kDa AnkG at the AIS and node, whereas myelinating glia express NF155 and 270/190-kDa AnkG or 220-kDa AnkB at paranodal junctions[30,35,36]. Together, these results demonstrate a remarkable example where two interacting proteins encoded by the same genes can be used by both neurons and myelinating glia as different isoforms for different functions.

DISCUSSION

Ankyrins organize membrane subdomains in diverse cell types and regulate cell-cell interactions through these domains[5,6]. Ankyrin and spectrin-based cytoskeletons also provide cells with membrane flexibility and toughness. For example, without functional AnkR, red blood cells become fragile, resulting in spherocytosis and anemia. In the nervous system, ankyrins and spectrins are reiteratively used to assemble polarized subdomains and support the delicate structure of axons and myelin[12,37–39]. Ankyrins were previously identified at paranodes[13,14], but their cellular source and functions remained unknown. Here, we showed that paranodal AnkB is produced by Schwann cells. However, this AnkB is dispensable for paranodal junction formation, function, and the organization of axonal membrane domains. In the CNS, AnkB is occasionally observed at paranodes. Instead, AnkG is enriched at both paranodes in oligodendrocytes and nodes of Ranvier in axons. Furthermore, the selective deletion of AnkG from myelinating glia caused a severe defect in paranodal junction formation during early development (Supplementary Fig. 2).

Our data show that paranodal ankyrins interact with NF155 *in vivo* to regulate the early phase of CNS paranodal junction assembly. The interaction between NFasc and ankyrins is required for aggregation of neuroblastoma cells mediated by homophilic NFasc interactions[25]. Disruption of NFasc's cytoplasmic interaction with ankyrins increases its lateral mobility and severely compromises the ability of NFasc-expressing cells to form

large aggregates[24,25]. Based on the multivalent binding property of ankyrins with more than one NFasc molecule and two ankyrin-binding sites on one spectrin tetramer, we speculate that interactions between NF155 and ankyrins stabilize many paranodal NF155 molecules in close proximity to one another to increase binding avidity for axonal Caspr/contactin.

Why do paranodal ankyrins play more important roles in the CNS than the PNS? In the CNS, paranodal junctions function as lateral diffusion barriers and are the primary mechanism responsible for clustering of AnkG, Nav channels, and βIV spectrin at nodes of Ranvier[23]. In contrast, paranodal junction formation in the PNS follows clustering of nodal proteins and plays a secondary role to that of heminodal clustering by gliomedin[4,40] (Supplementary Fig. 2b). This contrast may be partially explained by the observation that NF155 is expressed by oligodendrocytes before myelination, whereas Schwann cells express NF155 only after the onset of myelination and nodal protein clustering[27,36,41]. Similarly, paranodal clustering of ankyrins is detected during early myelination in the CNS[14], but only after Caspr clustering in the PNS[13]. Our results also suggest paranodal targeting of ankyrins does not require paranodal junctions or NF155. Based on these observations, we propose that during early CNS myelination, ankyrins facilitate the accumulation of NF155/Caspr/contactin clusters by actively targeting NF155 to paranodes, or by clustering and stabilizing the earliest NF155/Caspr/contactin complexes at paranodes. Without paranodal ankyrins in the CNS, paranodal junction formation is severely delayed and preceded by nodal clustering, similar to the normal situation in the PNS (Supplementary Fig. 2b). To further understand the molecular mechanisms by which ankyrins facilitate paranodal junction assembly, it will be important to determine the paranodal targeting mechanisms for AnkB and AnkG.

Although we observed a significant delay in CNS paranodal junction formation, our results show ankyrins are not absolutely required for junction assembly in the PNS or CNS. The eventual formation of paranodal junctions is not due to compensation by other ankyrins since neither AnkG nor AnkR compensates for the loss of AnkB in the PNS, and AnkR does not compensate for the loss of both AnkG and AnkB in the CNS (data not shown). We speculate that other unidentified glial paranodal junctional components may play a functional role redundant with that of ankyrins, or the clustering mechanism from the axonal paranodal cytoskeleton, including 4.1B and αII/βII spectrins[1,2,13], may be sufficient to sustain paranodal junction assembly. However, paranodal junctions still form in 4.1B- and βII spectrin-KO mice[17–19,42], consistent with the idea of robust and redundant mechanisms. To test this possibility, it will be necessary to generate mice lacking both paranodal ankyrins and 4.1B or βII spectrin to determine if they show more severe defects than single KO mice.

Alternatively, the local environment at paranodal junctions may be sufficient to support the slow maturation of junctional NF155/Caspr/contactin complexes. Mature paranodal junctions have lipid raft-like properties[27], and paranodal proteins have features characteristic of proteins often found in lipid rafts[43]. For example, contactin is a glycosylphosphatidylinositol-anchored protein and NFasc forms a dimer and is palmitoylated[44,45]. We previously proposed that when NF155 and Caspr/contactin complexes bind to each other at paranodes, lipid-raft lipid components are also recruited. The clustering of NF155/Caspr/contactin and lipid-raft lipid components mutually stabilize each other[27]. If this intrinsic mechanism is sufficient to constrain these CAMs within the

special paranodal lipid environment, removal of glial cytoskeletal scaffolds may only cause a delay in paranodal junction formation and no defects in maintenance. Nevertheless, our results show that in the CNS, these ankyrin-independent mechanisms can only rescue late paranodal junction formation.

Although ankyrins are common to almost every cell in multicellular organisms and function as scaffolds, expression of ankyrins is remarkably complicated. First, ankyrins can be transcribed from several different alternative promoters, and different first exons encode their own stretches of peptide sequences. Second, ankyrin transcripts undergo extensive alternative splicing to produce various ankyrin protein isoforms[5]. AnkB and AnkG have alternative long exons whose incorporation makes giant versions of ankyrins. Giant AnkB and AnkG were thought to be exclusive to neurons[5,6]. We consistently found myelinating glia utilize 220-kDa AnkB rather than its 440-kDa isoform. However, our analysis revealed that oligodendrocytes express both 190-kDa and 270-kDa AnkG. Why different ankyrin isoforms are expressed remains obscure since ankyrins generally function as scaffolds. However, one previous study showed that the protein domain specific to giant AnkG is required for its localization at the AIS[5], suggesting one purpose of the different isoforms may be to locate scaffolds in different membrane subdomains and perhaps also provide functional regulation for their assembly and maintenance. Future studies will be required to determine the functions of different ankyrin isoforms in these diverse cellular compartments.

AnkG has been implicated in psychiatric disorders including bipolar disorder, schizophrenia and autism by both association and sequencing studies[46–49]. In addition to its crucial role at the AIS and nodes in neurons, our study reveals the importance of glial AnkG, and this pool of AnkG must be considered while the psychiatric etiology of the probable “AnkG syndromes” is pursued. In spite of the severe delay in paranodal junction assembly and reduced conduction velocity in the *AnkG-cKO* and *AnkB/G-cKO* mice, we observed no obvious tremor or ataxia and many paranodal junctions had already formed by P21 (Figs. 3k and 4a). However, a more detailed behavioral analysis may reveal how proper paranodal junction assembly affects activity-dependent circuit refinement during development, since the temporal pattern of neural activity should be altered by the reduced action potential conduction velocity in the *AnkG-cKO* and *AnkB/G-cKO* neonates.

In conclusion, our study genetically defines paranodal ankyrins as ankyrins contributed by myelinating glia. Our data support a model where paranodal ankyrins facilitate clustering and stabilization of paranodal CAM complexes to potentiate early formation of paranodal junctions in the CNS.

METHODS

Animals

The AnkB conventional KO mice were described previously[15] except that the genetic background was changed to C57BL/6. The *Caspr*$^{-/-}$[29], *Ank3 exon 1b*$^{-/-}$[33], *Nfasc*$^{-/-}$[30,50] and *Cnp-Cre*[16] mice were described previously. Sprague-Dawley rats were purchased from Harlan Laboratories. *Ank2*^{floxed} mice were generated by the introduction of loxP sites flanking exon 24 of *Ank2* (ENSMUSE00001285026). The strategy results in the deletion of

73 bp of coding sequence: the splicing of exon 23 to exon 25 leads to a frame shift resulting in a premature stop codon in exon 25. Mice were crossed to generate pure lines of excised floxed mice devoid of the neomycin selection cassette. Mice were then screened by PCR and Southern analyses. *Ank3*^{floxed}: exons 23 and 24 (ENSMUSE00001261484 and ENSMUSE00001217354, respectively) are flanked by loxP sites[51]. *Nfasc*^{floxed} mice were kindly provided by Dr. Elior Peles (Weizmann Institute of Science, Rehovot, Israel) and will be described elsewhere. All experiments were performed in compliance with the National Institutes of Health Guide for the Care and Use of Laboratory Animals and were approved by the Baylor College of Medicine Institutional Animal Care and Use Committee.

Antibodies

The primary antibodies used were: rabbit antibodies against AnkB membrane-binding domain[12], AnkB C-terminal region (H-300, SantaCruz), AnkG spectrin-binding domain and C-terminal region[12], AnkG exon 1b and exon 1e (generated by immunizing against peptides unique to these domains followed by affinity purification of specific antibodies), AnkG 480/270[7] (generated, affinity purified, and kindly provided by Dr. Paul Jenkins, Duke University), AnkR (generated against His-tagged, full-length human AnkR and affinity purified), GFP (A11122, Life Technologies), NF-M (AB1987, EMD Millipore), Caspr[27], βIV spectrin SD[52], Kv1.2[53], Caspr2 (ab33994, Abcam), Nav1.2[54], Nav1.6[54], and 4.1G[55] (kindly provided by Dr. Elior Peles); mouse monoclonal antibodies against AnkB membrane-binding domain (N105/13 and N105/17, UC Davis/NIH NeuroMab Facility), AnkB spectrin-binding domain (2.20, SantaCruz), AnkG spectrin-binding domain or C-terminal region (N106/36 and N106/65, NeuroMab), Caspr (K65/35, NeuroMab), contactin (K73/20, NeuroMab), actin (C4, EMD Millipore), ZO-1 (ZO1-1A12, Life Technologies), E-cadherin (4A2C7, Life Technologies), Kv1.2 (K14/16, NeuroMab), Nav1.6 (K87A/10, NeuroMab), CNP (11-5B, Sigma-Aldrich), MAG (513, EMD Millipore), MBP (SMI-94, Covance), Necl4 (N244/5, NeuroMab), pan-Nav channels (K58/35[14]) and GFP (N86/38, NeuroMab); the rat monoclonal antibody against MBP (MAB386, EMD Millipore); chicken antibodies against NFasc (AF3235, R&D Systems) and βIV spectrin SD[56]; goat antibodies against contactin (AF904, R&D Systems), connexin 32 (C-20, Santa Cruz), and AnkG (generated against the C-terminal domain of AnkG minus the death domain and affinity purified). The secondary antibodies were purchased from Life Technologies and Jackson ImmunoResearch Laboratories.

DRG neuron-Schwann cell myelinating co-culture

Primary DRG neuron culture and Schwann cell culture were prepared from Sprague-Dawley rats as described previously[38]. The purified rat DRG neurons were infected with the adenovirus carrying the construct expressing AnkB shRNA and GFP[12] at 14 days *in vitro* (DIV). At 15 DIV, the whole culture medium was changed and the purified rat Schwann cells were added. Since 22 DIV, ascorbic acid had been included in the medium to induce myelination. The culture was fixed at 43 DIV (Fig. 1b, c) or 66 DIV (Fig. 1d) (21 or 44 days after induction of myelination, respectively) and immunostained. Under such conditions, transduced, myelinating Schwann cells were seldom observed. The DRG neurons of the AnkB conventional KO were prepared from P0 neonates. The purified rat Schwann cells

were added at 16 DIV; ascorbic acid had been included since 23 DIV. The co-culture was fixed and stained 28 days later (Fig. 1f).

Immunostaining was performed as described previously[23].

Electrophysiology

Compound action potentials were measured in a bath of Locke's solution with suction electrodes[14] or *in vivo*[57] as described.

Transmission electron microscopy was performed in Integrated Microscopy Core at Baylor College of Medicine as described prerviously[56]. The axon diameters were calculated by dividing the axon circumferences by π.

Immunoprecipitation

Adult rat sciatic nerves were homogenized in Homogenizing buffer (320 mM sucrose, 5 mM sodium phosphate pH 7.2, 0.2 mM NaF, 0.2 mM Na_3VO_4, 2 × PhosSTOP (Roche), 2 μg/ml aprotinin, 1 μg/ml leupeptin, 2 μg/ml antipain, 10 μg/ml benzamidine and 0.5 mM PMSF) with sonication. The supernatant was collected after 700 × g centrifugation for 10 min at 4°C. P21 mouse spinal cords were homogenized in Homogenizing buffer with Dounce homogenizer. The supernatant from 700 × g centrifugation (10 min at 4°C) was centrifuged again at 27200 × g for 90 min at 4°C. The pellet was resuspended in Homogenizing buffer. The lysates used for immunoprecipitation were prepared by diluting sciatic nerve and spinal cord homogenates to final protein concentration at 1 mg/ml with Lysis buffer (1% (v/v) Triton X-100, 20 mM Tris-HCl pH 8.0, 10 mM EDTA, 150 mM NaCl, 10 mM NaN_3, 2 × PhosSTOP, 2 μg/ml aprotinin, 1 μg/ml leupeptin, 2 μg/ml antipain, 10 μg/ml benzamidine and 0.5 mM PMSF), supplementing Triton X-100 to totally 1%, mixing by a rotator for 1 hr at 4°C, centrifuging at 13000 × g for 30 min at 4°C and harvesting the supernatants. 16 μg of mouse monoclonal anti-AnkB N105/17 and anti-GFP N86/38 antibodies (for sciatic nerves) and 16 μg of mouse monoclonal anti-AnkG N106/36 and anti-GFP N86/38 antibodies (for spinal cords) were each incubated with 40 μl of protein A agarose (Thermo Scientific) in 300 μl of Lysis buffer for 1–2 hr. The beads were washed with 1 ml of Lysis buffer three times and then incubated with the lysates (650 μl for sciatic nerves and 620 μl for spinal cords) overnight at 4°C. The beads were then washed with 1 ml of ice-cold Lysis buffer four times and subjected to Western blotting.

Preparation of tissue homogenates

Sciatic nerve homogenates and spinal cord membrane homogenates were prepared as described in Immunoprecipitation. Optic nerve homogenates were prepared as described for sciatic nerve homogenates.

Reverse transcription-quantitative polymerase chain reaction (RT-qPCR)

Total RNA of P31 spinal cords and sciatic nerves were prepared by homogenizing tissues in TRIzol reagent (Life Technologies) and then purifying RNA with Direct-zol RNA MiniPrep (Zymo Research). 1 μg (from spinal cords) and 0.5–0.64 μg (from sciatic nerves) of total RNA were used in 20 μl of reverse transcription reaction with SuperScript III First-Strand

Synthesis System (Life Technologies) with random hexamers in the presence or absence of the reverse transcriptase according to the manufacturer's instruction. The RT reaction was then diluted to 1/4 × and 2 μl were used for qPCR in 25 μl of reaction with Power SYBR Green PCR Master Mix and StepOnePlus Real-Time PCR System (both from Life Technologies). The primers used in qPCR are as follows (sequences shown from 5′ to 3′): AnkB exon 24 (forward: ACCACTACCACGACTATCAC; reverse: GTAGTTCATGCCATCCAGG), AnkB 440-kDa (forward: GGAACCCAAATCCACAAGAG ; reverse: ACAGGAACTTCATTAACCAGG), AnkB 220-kDa (forward: CAACTTAAACATCACCCTGC ; reverse: AGTTCTCTTGCTAATTCTGTCC), AnkB exon 1″ (forward: ACCGAGGGAAGGAGTTC; reverse: GGAGAGCATTGAGTCCATTC), AnkB exon 1′ (forward: GCACATGGATTACAGTCTGAG; reverse: GCAGTTCTTCATGTCCCTG), AnkB exon 1 (forward: CTTCCCAAACTGTTCAAAATG; reverse: CCCCTTTCAGATATTCCACC), AnkB exon '1 (forward: GGATGGAGCGGAAAAGAAA; reverse: CAGGTGGAGAGCATTGAG), AnkG exon 23 (forward: GTGAATGGGAACACAGCTC; reverse: TCATCGTTTCTGGGACATTC), AnkG exon 1a (forward: GCAGAGCCGAGTTCCTG; reverse: TGAATAACAGGATCCAAAGTCAC), AnkG exon 1e (forward: GTGAAGAGCCAAAGGAGAAG; reverse: TTGGAAGCAAGATGGAGTG), AnkG exon 1b (forward: AAAAGGAAACACCGCAAACG; reverse: CTCAGAGACCACTTCCACATG), AnkG 480-kDa (forward: AGTAGGAGGACTGGTCCG; reverse: AGTTGTGGCATTCTTTCCG), AnkG 270-kDa (forward: GCCATGTCTCCAGATGTTG; reverse: TCTGTCCAACTAAGTCCCAG), AnkG 190-kDa (forward: CTTTGCCTCCCTAGCTTTAC; reverse: the same as 270), and Polr2a (forward: CATCAAGAGAGTGCAGTTCG; reverse: CCATTAGTCCCCCAAGTTTG). Polr2a was chosen as the internal control[58]. The efficiency of all the primer pairs was validated to be between 90% and 103% on six points of 4-fold serial dilutions of adult mouse brain cDNAs. The specificity was confirmed by gel electrophoresis and sequencing from both ends of the PCR products. Technical triplicates of each set of *WT*, *cHet* and *cKO* tissues and three to four biological replicates (specified in the figure legends) were performed and analyzed. Comparison of *cHet* with *WT* and *cKO* with *cHet* was carried out by one-sample two-tailed *t* tests and two-sample two-tailed *t* tests, respectively.

Statistics

No statistical methods were used to pre-determine sample sizes, but our sample sizes are similar to those reported previously[23]. Except for electrophysiological recordings, data collection and analysis were not performed blind to the conditions of the experiments. Sets of age-matched cKO or KO mice and their controls were randomly collected from littermates or from two litters which had closer dates of birth. Normality of the P56 *WT* and *AnkB-cKO* sciatic nerve conduction velocities was tested and not rejected by the Shapiro-Wilk tests: *WT*: $W(5) = 0.956$, $p = 0.782$; *AnkB-cKO*: $W(6) = 0.878$, $p = 0.259$. For other data compared by *t* tests, the distributions were assumed to be normal. A supplementary methods checklist is available online in the supplementary information.

Supplementary Material

Refer to Web version on PubMed Central for supplementary material.

Acknowledgments

This work was supported by grants from the NIH (NS069688 (MNR), NS044916 (MNR), HL084583 (PJM), HL083422 (PJM), HL114383 (PJM)), the National Multiple Sclerosis Society, and the Dr. Miriam and Sheldon G. Adelson Medical Research Foundation. V. Bennett is an investigator of the Howard Hughes Medical Institute.

References

1. Poliak S, Peles E. The local differentiation of myelinated axons at nodes of Ranvier. Nat Rev Neurosci. 2003; 4:968–980. [PubMed: 14682359]
2. Salzer JL. Polarized domains of myelinated axons. Neuron. 2003; 40:297–318. [PubMed: 14556710]
3. Babbs CF, Shi R. Subtle paranodal injury slows impulse conduction in a mathematical model of myelinated axons. PLoS One. 2013; 8:e67767. [PubMed: 23844090]
4. Chang KJ, Rasband MN. Excitable domains of myelinated nerves: axon initial segments and nodes of Ranvier. Curr Top Membr. 2013; 72:159–192. [PubMed: 24210430]
5. Bennett V, Lorenzo DN. Spectrin- and ankyrin-based membrane domains and the evolution of vertebrates. Curr Top Membr. 2013; 72:1–37. [PubMed: 24210426]
6. Bennett V, Healy J. Membrane domains based on ankyrin and spectrin associated with cell-cell interactions. Cold Spring Harb Perspect Biol. 2009; 1:a003012. [PubMed: 20457566]
7. Kordeli E, Lambert S, Bennett V. Ankyrin$_G$. A new ankyrin gene with neural-specific isoforms localized at the axonal initial segment and node of Ranvier. J Biol Chem. 1995; 270:2352–2359. [PubMed: 7836469]
8. Dzhashiashvili Y, et al. Nodes of Ranvier and axon initial segments are ankyrin G-dependent domains that assemble by distinct mechanisms. J Cell Biol. 2007; 177:857–870. [PubMed: 17548513]
9. Rasband MN. The axon initial segment and the maintenance of neuronal polarity. Nat Rev Neurosci. 2010; 11:552–562. [PubMed: 20631711]
10. Gasser A, et al. An ankyrinG-binding motif is necessary and sufficient for targeting $Na_V1.6$ sodium channels to axon initial segments and nodes of Ranvier. J Neurosci. 2012; 32:7232–7243. [PubMed: 22623668]
11. Chan W, Kordeli E, Bennett V. 440-kD ankyrin$_B$: structure of the major developmentally regulated domain and selective localization in unmyelinated axons. J Cell Biol. 1993; 123:1463–1473. [PubMed: 8253844]
12. Galiano MR, et al. A distal axonal cytoskeleton forms an intra-axonal boundary that controls axon initial segment assembly. Cell. 2012; 149:1125–1139. [PubMed: 22632975]
13. Ogawa Y, et al. Spectrins and ankyrinB constitute a specialized paranodal cytoskeleton. J Neurosci. 2006; 26:5230–5239. [PubMed: 16687515]
14. Rasband MN, et al. Dependence of nodal sodium channel clustering on paranodal axoglial contact in the developing CNS. J Neurosci. 1999; 19:7516–7528. [PubMed: 10460258]
15. Scotland P, Zhou D, Benveniste H, Bennett V. Nervous system defects of Ankyrin$_B$ (−/−) mice suggest functional overlap between the cell adhesion molecule L1 and 440-kD Ankyrin$_B$ in premyelinated axons. J Cell Biol. 1998; 143:1305–1315. [PubMed: 9832558]
16. Lappe-Siefke C, et al. Disruption of *Cnp1* uncouples oligodendroglial functions in axonal support and myelination. Nat Genet. 2003; 33:366–374. [PubMed: 12590258]
17. Horresh I, Bar V, Kissil JL, Peles E. Organization of myelinated axons by Caspr and Caspr2 requires the cytoskeletal adapter protein 4.1B. J Neurosci. 2010; 30:2480–2489. [PubMed: 20164332]

18. Cifuentes-Diaz C, et al. Protein 4.1B contributes to the organization of peripheral myelinated axons. PLoS One. 2011; 6:e25043. [PubMed: 21966409]
19. Zhang C, Susuki K, Zollinger DR, Dupree JL, Rasband MN. Membrane domain organization of myelinated axons requires βII spectrin. J Cell Biol. 2013; 203:437–443. [PubMed: 24217619]
20. Rios JC, et al. Paranodal interactions regulate expression of sodium channel subtypes and provide a diffusion barrier for the node of Ranvier. J Neurosci. 2003; 23:7001–7011. [PubMed: 12904461]
21. Hoshi T, et al. Nodal protrusions, increased Schmidt-Lanterman incisures, and paranodal disorganization are characteristic features of sulfatide-deficient peripheral nerves. Glia. 2007; 55:584–594. [PubMed: 17299768]
22. Cahoy JD, et al. A transcriptome database for astrocytes, neurons, and oligodendrocytes: a new resource for understanding brain development and function. J Neurosci. 2008; 28:264–278. [PubMed: 18171944]
23. Susuki K, et al. Three mechanisms assemble central nervous system nodes of Ranvier. Neuron. 2013; 78:469–482. [PubMed: 23664614]
24. Garver TD, Ren Q, Tuvia S, Bennett V. Tyrosine phosphorylation at a site highly conserved in the L1 family of cell adhesion molecules abolishes ankyrin binding and increases lateral mobility of neurofascin. J Cell Biol. 1997; 137:703–714. [PubMed: 9151675]
25. Tuvia S, Garver TD, Bennett V. The phosphorylation state of the FIGQY tyrosine of neurofascin determines ankyrin-binding activity and patterns of cell segregation. Proc Natl Acad Sci U S A. 1997; 94:12957–12962. [PubMed: 9371782]
26. Jenkins SM, et al. FIGQY phosphorylation defines discrete populations of L1 cell adhesion molecules at sites of cell-cell contact and in migrating neurons. J Cell Sci. 2001; 114:3823–3835. [PubMed: 11719549]
27. Schafer DP, Bansal R, Hedstrom KL, Pfeiffer SE, Rasband MN. Does paranode formation and maintenance require partitioning of neurofascin 155 into lipid rafts? J Neurosci. 2004; 24:3176–3185. [PubMed: 15056697]
28. Bhat MA, et al. Axon-glia interactions and the domain organization of myelinated axons requires neurexin IV/Caspr/Paranodin. Neuron. 2001; 30:369–383. [PubMed: 11395000]
29. Gollan L, Salomon D, Salzer JL, Peles E. Caspr regulates the processing of contactin and inhibits its binding to neurofascin. J Cell Biol. 2003; 163:1213–1218. [PubMed: 14676309]
30. Zonta B, et al. Glial and neuronal isoforms of Neurofascin have distinct roles in the assembly of nodes of Ranvier in the central nervous system. J Cell Biol. 2008; 181:1169–1177. [PubMed: 18573915]
31. Kunimoto M. A neuron-specific isoform of brain ankyrin, 440-kD ankyrin$_B$, is targeted to the axons of rat cerebellar neurons. J Cell Biol. 1995; 131:1821–1829. [PubMed: 8557748]
32. Cunha SR, Le Scouarnec S, Schott JJ, Mohler PJ. Exon organization and novel alternative splicing of the human *ANK2* gene: implications for cardiac function and human cardiac disease. J Mol Cell Cardiol. 2008; 45:724–734. [PubMed: 18790697]
33. Zhou D, et al. Ankyrin$_G$ is required for clustering of voltage-gated Na channels at axon initial segments and for normal action potential firing. J Cell Biol. 1998; 143:1295–1304. [PubMed: 9832557]
34. Rueckert EH, et al. *Cis*-acting regulation of brain-specific *ANK3* gene expression by a genetic variant associated with bipolar disorder. Mol Psychiatry. 2013; 18:922–929. [PubMed: 22850628]
35. Davis JQ, Lambert S, Bennett V. Molecular composition of the node of Ranvier: identification of ankyrin-binding cell adhesion molecules neurofascin (mucin+/third FNIII domain-) and NrCAM at nodal axon segments. J Cell Biol. 1996; 135:1355–1367. [PubMed: 8947556]
36. Tait S, et al. An oligodendrocyte cell adhesion molecule at the site of assembly of the paranodal axo-glial junction. J Cell Biol. 2000; 150:657–666. [PubMed: 10931875]
37. Susuki K, Rasband MN. Spectrin and ankyrin-based cytoskeletons at polarized domains in myelinated axons. Exp Biol Med (Maywood). 2008; 233:394–400. [PubMed: 18367627]
38. Susuki K, et al. Schwann cell spectrins modulate peripheral nerve myelination. Proc Natl Acad Sci U S A. 2011; 108:8009–8014. [PubMed: 21518878]
39. Hammarlund M, Jorgensen EM, Bastiani MJ. Axons break in animals lacking β-spectrin. J Cell Biol. 2007; 176:269–275. [PubMed: 17261846]

40. Feinberg K, et al. A glial signal consisting of gliomedin and NrCAM clusters axonal Na^+ channels during the formation of nodes of Ranvier. Neuron. 2010; 65:490–502. [PubMed: 20188654]
41. Eisenbach M, et al. Differential clustering of Caspr by oligodendrocytes and Schwann cells. J Neurosci Res. 2009; 87:3492–3501. [PubMed: 19565653]
42. Einheber S, et al. The 4.1B cytoskeletal protein regulates the domain organization and sheath thickness of myelinated axons. Glia. 2013; 61:240–253. [PubMed: 23109359]
43. Munro S. Lipid rafts: elusive or illusive? Cell. 2003; 115:377–388. [PubMed: 14622593]
44. Zhang X, Davis JQ, Carpenter S, Bennett V. Structural requirements for association of neurofascin with ankyrin. J Biol Chem. 1998; 273:30785–30794. [PubMed: 9804856]
45. Ren Q, Bennett V. Palmitoylation of neurofascin at a site in the membrane-spanning domain highly conserved among the L1 family of cell adhesion molecules. J Neurochem. 1998; 70:1839–1849. [PubMed: 9572267]
46. Shi L, et al. Whole-genome sequencing in an autism multiplex family. Mol Autism. 2013; 4:8. [PubMed: 23597238]
47. Iqbal Z, et al. Homozygous and heterozygous disruptions of *ANK3*: at the crossroads of neurodevelopmental and psychiatric disorders. Hum Mol Genet. 2013; 22:1960–1970. [PubMed: 23390136]
48. Yuan A, et al. *ANK3* as a risk gene for schizophrenia: new data in Han Chinese and meta analysis. Am J Med Genet B Neuropsychiatr Genet. 2012; 159B:997–1005. [PubMed: 23109352]
49. Leussis MP, Madison JM, Petryshen TL. Ankyrin 3: genetic association with bipolar disorder and relevance to disease pathophysiology. Biol Mood Anxiety Disord. 2012; 2:18. [PubMed: 23025490]
50. Sherman DL, et al. Neurofascins are required to establish axonal domains for saltatory conduction. Neuron. 2005; 48:737–742. [PubMed: 16337912]
51. Jenkins PM, et al. E-cadherin polarity is determined by a multifunction motif mediating lateral membrane retention through ankyrin-G and apical-lateral transcytosis through clathrin. J Biol Chem. 2013; 288:14018–14031. [PubMed: 23530049]
52. Yang Y, Lacas-Gervais S, Morest DK, Solimena M, Rasband MN. βIV spectrins are essential for membrane stability and the molecular organization of nodes of Ranvier. J Neurosci. 2004; 24:7230–7240. [PubMed: 15317849]
53. Rhodes KJ, Keilbaugh SA, Barrezueta NX, Lopez KL, Trimmer JS. Association and colocalization of K^+ channel α- and β-subunit polypeptides in rat brain. J Neurosci. 1995; 15:5360–5371. [PubMed: 7623158]
54. Schafer DP, Custer AW, Shrager P, Rasband MN. Early events in node of Ranvier formation during myelination and remyelination in the PNS. Neuron Glia Biol. 2006; 2:69–79. [PubMed: 16652168]
55. Ivanovic A, et al. The cytoskeletal adapter protein 4.1G organizes the internodes in peripheral myelinated nerves. J Cell Biol. 2012; 196:337–344. [PubMed: 22291039]
56. Chang KJ, Susuki K, Dours-Zimmermann MT, Zimmermann DR, Rasband MN. Oligodendrocyte myelin glycoprotein does not influence node of Ranvier structure or assembly. J Neurosci. 2010; 30:14476–14481. [PubMed: 20980605]
57. Susuki K, et al. Gangliosides contribute to stability of paranodal junctions and ion channel clusters in myelinated nerve fibers. Glia. 2007; 55:746–757. [PubMed: 17352383]
58. Radoni A, et al. Guideline to reference gene selection for quantitative real-time PCR. Biochem Biophys Res Commun. 2004; 313:856–862. [PubMed: 14706621]

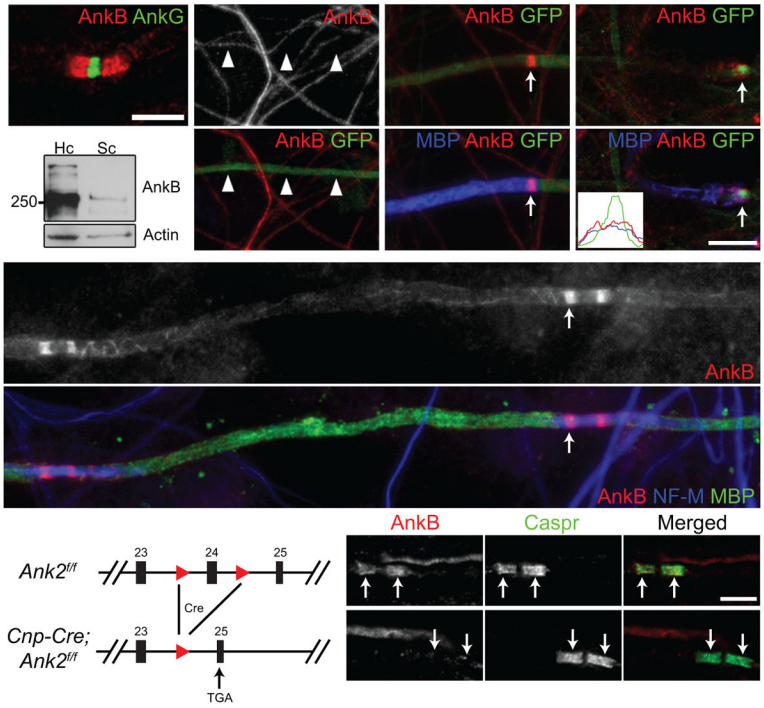

Figure 1.

Paranodal AnkB is derived from Schwann cells in the PNS. (**a**) Immunostaining of a mouse sciatic nerve for AnkG (node, rabbit polyclonal anti-AnkG) and AnkB (paranodes, N105/17). (**b**) Cultured DRG neurons were infected with adenovirus carrying a GFP and AnkB shRNA-expressing construct, and immunostained (AnkB, N105/13). Arrowheads point to the GFP-positive axon. (**c, d**) Schwann cells were added to the same culture as in (**b**) and induced to myelinate. The co-culture was labeled for myelin basic protein (MBP), GFP and AnkB (N105/13 (**c**) or N105/17 (**d**)). The arrows point to paranodal AnkB. A line scan of fluorescence intensity of the paranode indicated in (**d**) is shown in the inset. (**e**) Immunoblots of lysates from rat hippocampal (Hc) neuron and purified Schwann cell (Sc) cultures (AnkB, N105/17). The full blots are presented in Supplementary Fig. 3. (**f**) DRG neurons from the AnkB conventional KO were co-cultured with myelinating rat Schwann cells and immunostained for AnkB (N105/17), neurofilament-M (NF-M) and MBP. The arrow points to a paranode. Localization of AnkB along the inner mesaxon[13] was also observed as spiral extensions from paranodal junctions. (**g**) The scheme of the *Ank2* conditional allele. The two loxP sites (red triangles) flank exon 24. After Cre recombination and removal of exon 24, a premature stop codon is generated in exon 25. (**h, i**) Immunostaining of 4-week-old *AnkB-cHet* (**h**) and *AnkB-cKO* (**i**) sciatic nerves (AnkB, rabbit polyclonal anti-AnkB). Arrows point to paranodal junctions. Scale bars = 5 μm (**a; h, i**), and 10 μm (**b–d, f**).

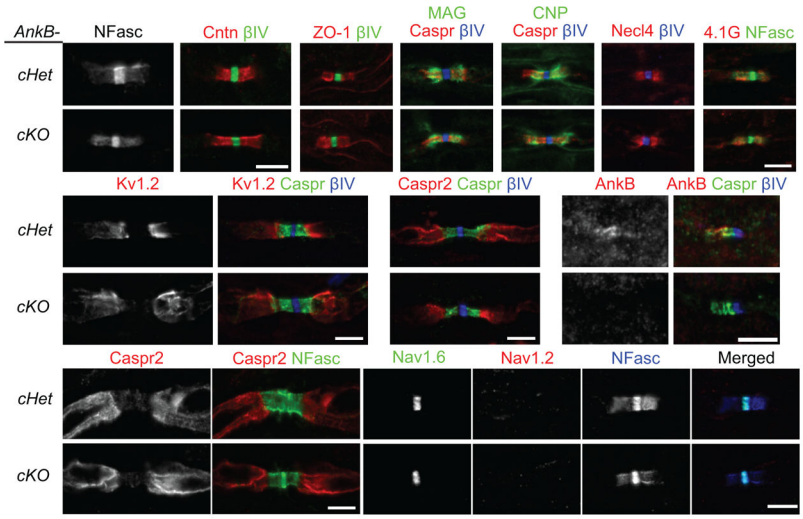

Figure 2.

No paranodal or axonal abnormalities were observed in sciatic nerves of *AnkB-cKO* mice. (**a–l**) Immunostaining of sciatic nerve longitudinal sections from 4 to 6-week-old (**a–i, l**), P3 (**j**, AnkB, N105/17) and 1-year-old (**k**) mice shows normal paranodal and juxtaparanodal domains and proper Nav channel subtype switch in *AnkB-cKO* mice. NFasc, neurofascin (both nodal 186-kDa and paranodal 155-kDa isoforms were stained). Cntn, contactin. βIV, βIV spectrin. ZO-1, zona occludens protein 1. MAG, myelin-associated glycoprotein. CNP, 2′,3′-cyclic nucleotide 3′ phosphodiesterase. Necl4, nectin-like protein 4. Two mice per genotype and more than 75 (**j**) or 150 (**a–i, k, l**) nodes were examined in each mouse. Scale bars = 5 μm (**a, b; c–g; h; i; j; k; l**).

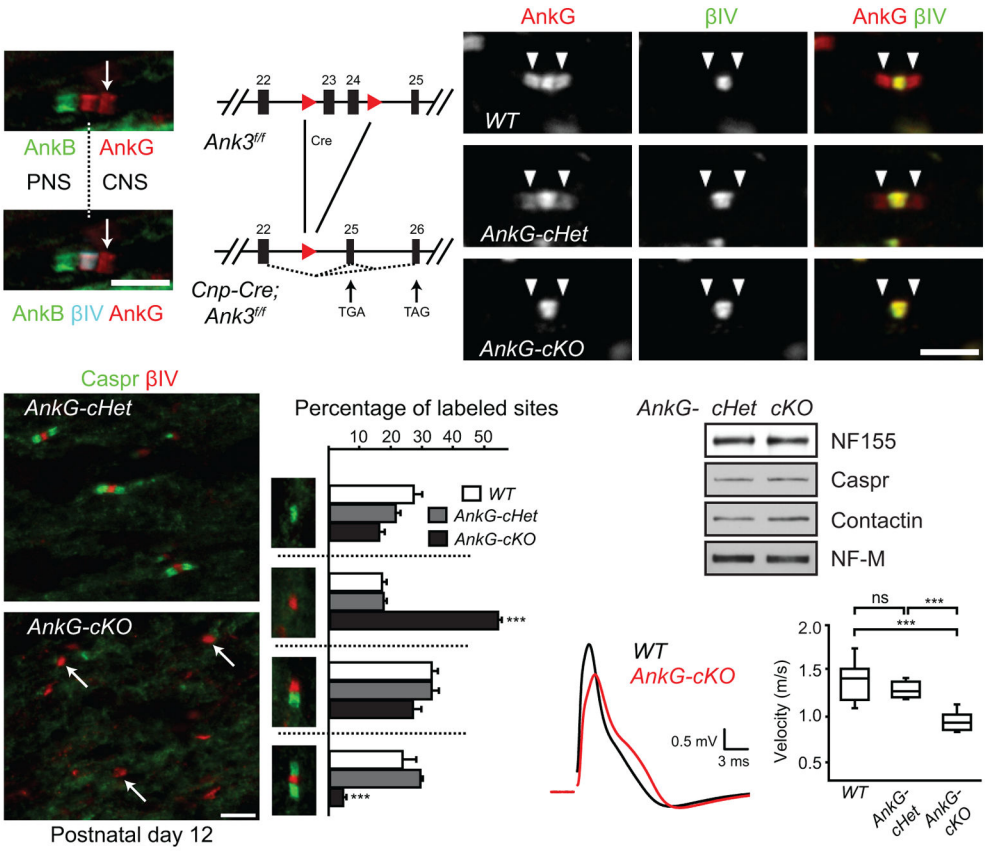

Figure 3.

Paranodal junction assembly is disrupted in *AnkG-cKO* mice. (**a**) The dorsal root entry zone from a P7 mouse spinal cord immunostained for AnkB (N105/13), AnkG (N106/36) and βIV spectrin. The dotted line indicates the transition from PNS to CNS. The arrow points to the CNS paranode. (**b**) The scheme of the *Ank3* conditional allele. The two loxP sites (red triangles) flank exons 23 and 24. After Cre recombination, a premature stop codon is generated in exon 25 or 26. (**c–e**) Immunostaining of P22 optic nerves (AnkG, N106/65). Arrowheads point to paranodes. (**f, g**) Immunostaining of P12 optic nerves. Arrows point to three nodal clusters without accompanying paranodal junctions. (**h**) Percentages of full nodes and nodal intermediates in P12 optic nerves (N = 3 for all genotypes). Unpaired two-tailed *t* tests (*cKO* vs. *cHet*): nodes alone: $p = 0.000003$; full nodes: $p = 0.00001$. The bar graphs show mean + SEM. ***, $p < 0.001$. (**i**) Immunoblots of P12 optic nerve homogenates. The full blots are presented in Supplementary Fig. 4. (**j, k**) Conduction of P17 optic nerves was measured using suction electrodes. N = 8 for *WT* and *AnkG-cKO*; N = 6 for *AnkG-cHet*. Two-tailed Mann-Whitney tests: *WT* vs. *cHet:* $p = 0.282$; *WT* vs. *cKO:* $p = 0.0003$; *cHet* vs. *cKO:* $p = 0.0007$. Data are shown in box-and-whisker plots (maximum, 75th percentile, median, 25th percentile, and minimum are shown). ***, $p < 0.001$; ns, not significant. Scale bars = 5 μm (**a; f, g**); 3 μm (**c–e**).

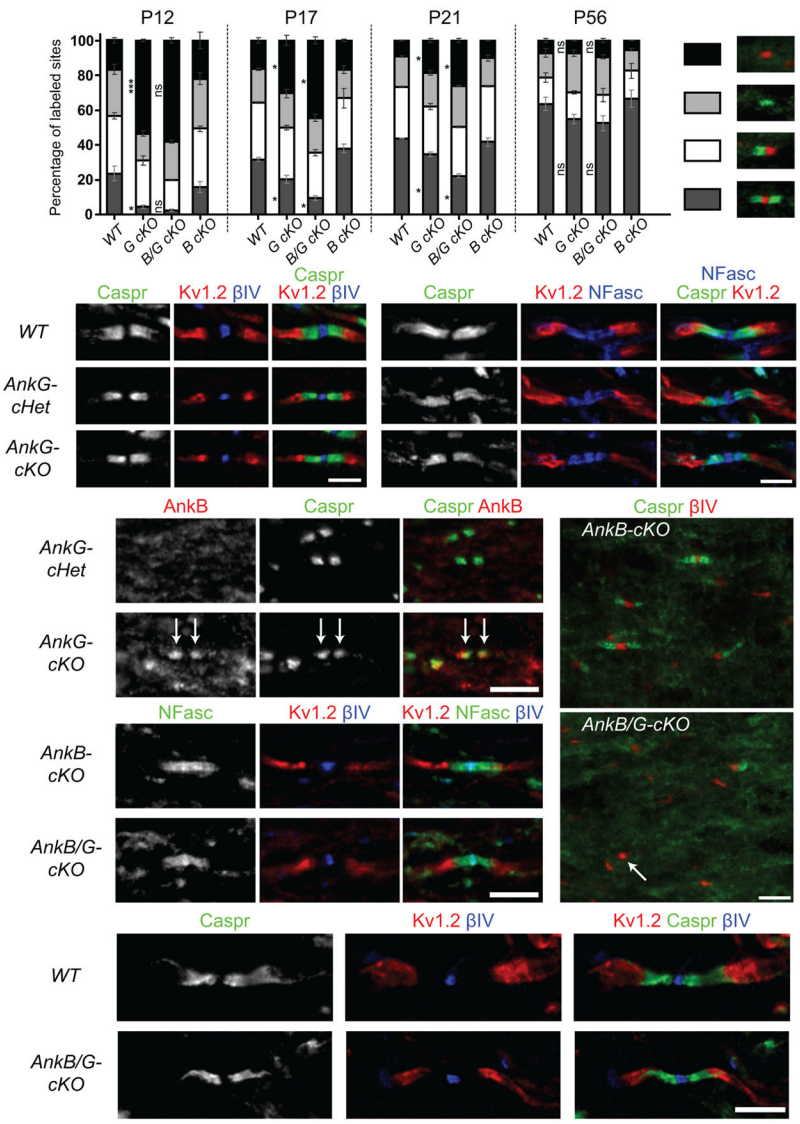

Figure 4.

Paranodal junctions recover over time in the CNS of the *AnkG-cKO* and *AnkB/G-cKO* mice. (**a**) Percentages of full nodes and nodal intermediates in P12, P17, P21 and P56 optic nerves. *WT*, wild type. *G cKO*, *AnkG-cKO*. *B cKO*, *AnkB-cKO*. *B/G cKO*, *AnkB/G-cKO*. The data for P12 *WT* and *G cKO* are the same as those shown in Fig. 3h. N = 2 mice for *AnkB/G-cKO* at P12, *AnkB-cKO* at P17 and all the genotypes at P21; N = 3 mice for the others. 200–500 sites per animal at P12 and 600–1400 at P17–P56 were counted. Unpaired two-tailed *t* tests: ***, $p < 0.001$; *, $p < 0.05$; ns, not significant (for exact *p* values, please see the supplementary methods checklist). The bar graphs show mean ± SEM. (**b–k**) Immunostaining of optic nerves from P22 (**b, d, e**), 1-year-old (**c, j, k**), P12 (**f, i**) and P21 (**g, h**) mice with antibodies as indicated. The anti-AnkB N105/17 was used in (**d, e**). The arrows in (**e**) point to paranodal AnkB; the arrow in (**i**) points to one nodal cluster of βIV spectrin without accompanying paranodal junctions. At least two mice per genotype and more than

150 nodes of each mouse were examined. Scale bars = 3 μm (**b; c**), and 5 μm (**d–e; f, i; g–h; j–k**).

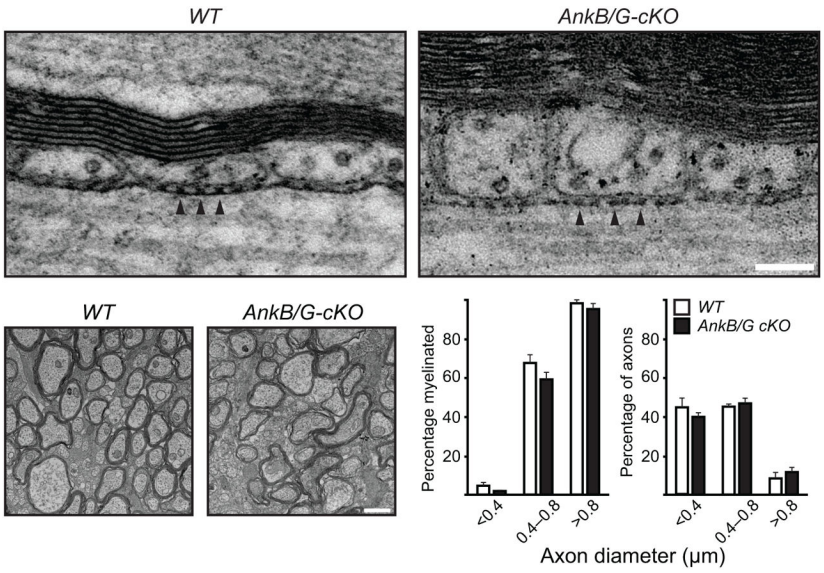

Figure 5.

Paranodal junction assembly and myelination proceed in the absence of both AnkB and AnkG in oligodendrocytes. (**a**) Electron micrographs of adult optic nerve longitudinal sections. Arrowheads point to the transverse bands. (**b**) Electron micrographs of P17 optic nerve cross sections. (**c**) Percentage of axons in each diameter range that were myelinated. (**d**) Percentage of total axons that belonged to different groups of diameter ranges. N = 3 for each genotype shown in (**c, d**). The bar graphs show mean + SEM. Scale bars = 100 nm (**a**) and 1 μm (**b**).

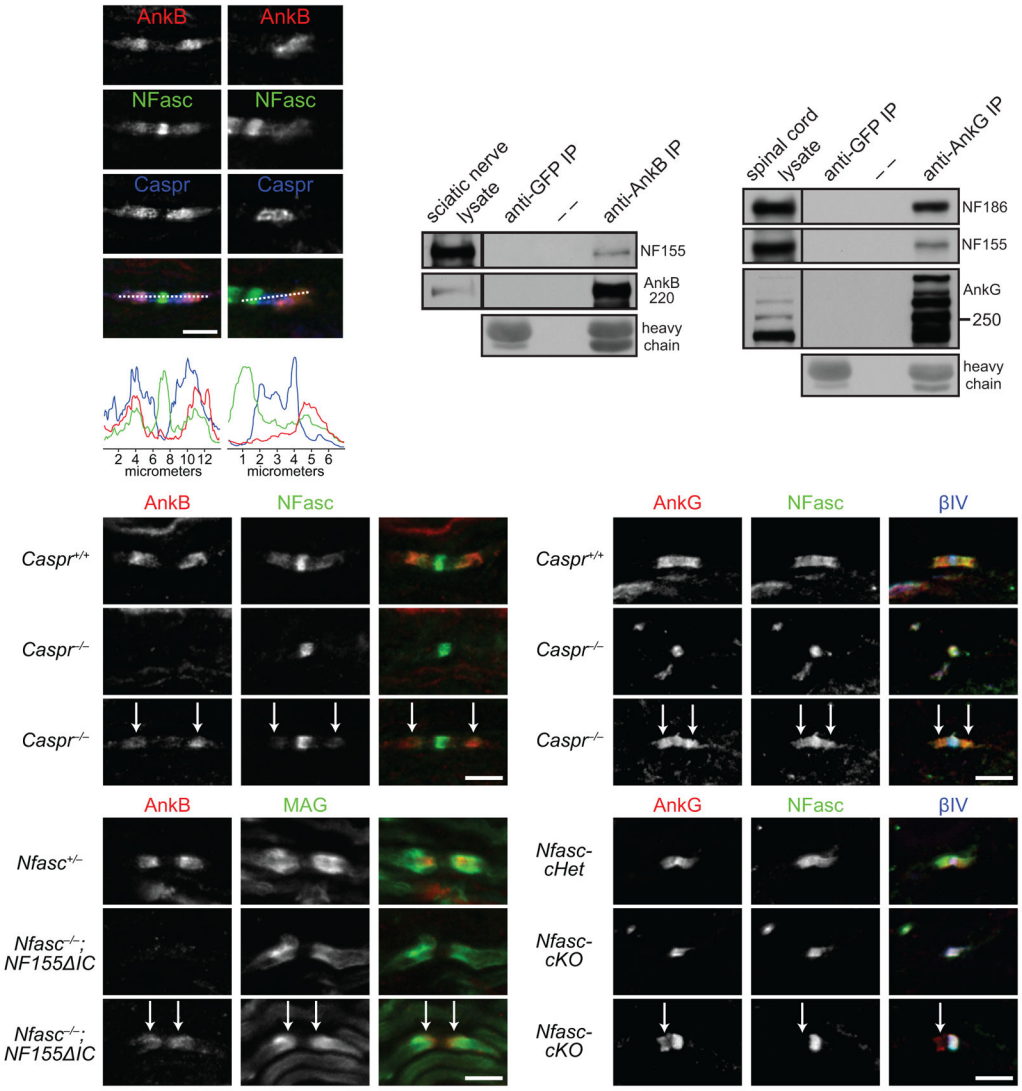

Figure 6.

AnkB and AnkG interact with NF155 *in vivo* and can be targeted to paranodes independently of paranodal junctions and NF155. (**a–d**) P8 sciatic nerve sections were stained for AnkB (N105/17), NFasc and Caspr (**a, b**), and the respective longitudinal line scans are shown (**c, d**). (**e**) Immunoprecipitation of AnkB from adult rat sciatic nerves co-precipitated NF155. Immunoprecipitation with the anti-GFP antibody served as a negative control. Heavy chain, mouse IgG heavy chain. AnkB was detected by H-300 rabbit polyclonal antibodies. (**f**) Immunoprecipitation of AnkG from P21 mouse spinal cords co-precipitated NF186 and NF155. AnkG was detected by the goat polyclonal antibodies. The immunoprecipitation in (**e, f**) was reproduced at least three times. The full blots are presented in Supplementary Fig. 3. (**g–i**) Immunostaining of P7 sciatic nerves (AnkB, rabbit polyclonal). Arrows point to the residual AnkB and NFasc at paranodes. (**j–l**) Immunostaining of P7 spinal cords (AnkG, N106/36). Arrows point to the residual AnkG and NFasc at paranodes. (**m–o**) Immunostaining of P5 sciatic nerves (AnkB, rabbit polyclonal). Arrows point to the paranodes with residual AnkB. (**p–r**) Immunostaining of

P12 *Nfasc-cHet* (*Cnp-Cre;Nfasc*$^{f/+}$) and *Nfasc-cKO* (*Cnp-Cre;Nfasc*$^{f/f}$) spinal cords (AnkG, N106/36). Two mice per genotype and more than 100 nodes were examined in each mouse. 80–190 nodes per animal were quantified. Scale bars = (**a, b**) 5 μm for (a) and 3.3 μm for (b); 5 μm (**g–i**, **j–l**, **m–o**, and **p–r**).

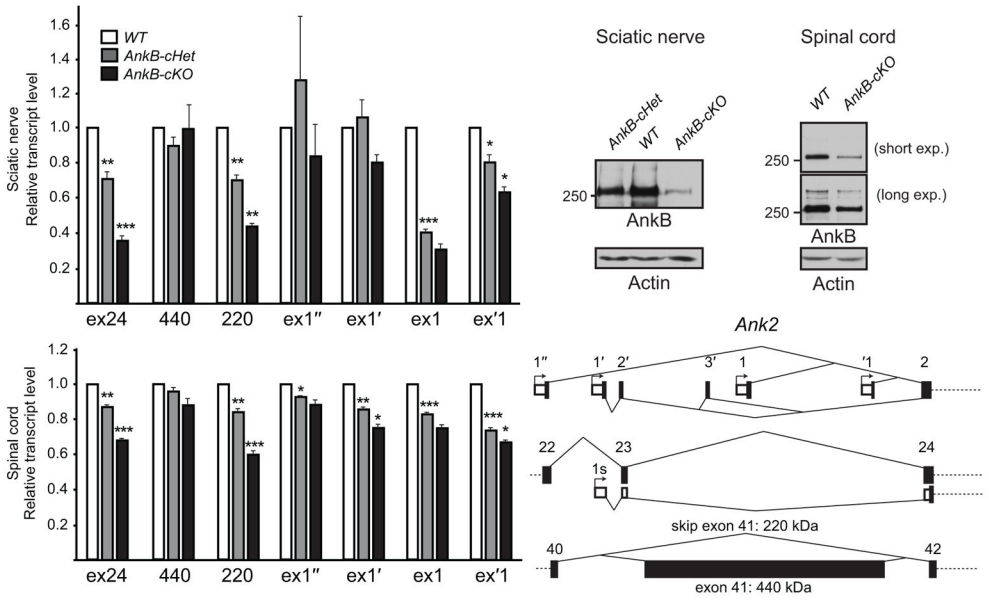

Figure 7.

Schwann cells and oligodendrocytes express 220-kDa isoform of AnkB from multiple promoters. (**a**) RT-qPCR analysis of P31 sciatic nerves shows the transcript levels relative to *WT* after normalization to Polr2a as the internal control. N = 4 for all genotypes analyzed. Unpaired two-tailed *t* tests (1 vs. *cHet*, one-sample; *cHet* vs. *cKO*, two-sample, respectively): *, $p < 0.05$; **, $p < 0.01$; ***, $p < 0.001$ (for exact *p* values, please see the supplementary methods checklist). The bar graphs show mean + SEM. (**b**) Immunoblots of adult sciatic nerve homogenates probed for AnkB (H-300 rabbit antibody) and actin. (**c**) Immunoblots of membrane homogenates from P42 spinal cords probed for AnkB (N105/17) and actin. The full blots in (**b, c**) are presented in Supplementary Fig. 4. (**d**) RT-qPCR analysis of P31 spinal cords shows the transcript levels relative to *WT* after normalization to Polr2a as the internal control. N = 4 for all genotypes analyzed. Unpaired two-tailed *t* tests (1 vs. *cHet*, one-sample; *cHet* vs. *cKO*, two-sample, respectively): *, $p < 0.05$; **, $p < 0.01$; ***, $p < 0.001$ (for exact *p* values, please see the supplementary methods checklist). The bar graphs show mean + SEM. (**e**) The schema shows the alternative first exons from different promoters and alternative splicing of exon 41 of *Ank2*.

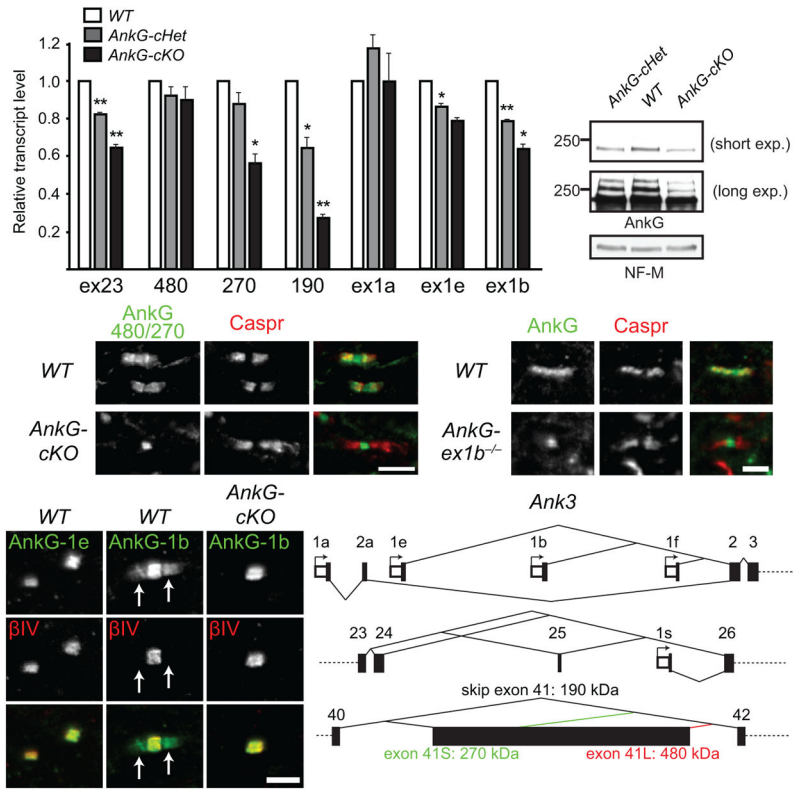

Figure 8.

Oligodendrocytes express the 270-kDa and 190-kDa isoforms of AnkG from the promoter upstream to exon 1b. (**a**) RT-qPCR analysis of P31 spinal cords shows the transcript levels relative to *WT* after normalization to Polr2a as the internal control. N = 3 for all genotypes analyzed. Unpaired two-tailed *t* tests (1 vs. *cHet*, one-sample; *cHet* vs. *cKO*, two-sample, respectively): *, $p < 0.05$; **, $p < 0.01$ (for exact *p* values, please see the supplementary methods checklist). The bar graphs show mean + SEM. (**b**) Immunoblots of membrane homogenates from P31 spinal cords probed for AnkG (goat polyclonal antibody) and NF-M. The full blots are presented in Supplementary Fig. 4. (**c**) Immunostaining of P12 spinal cords with antibodies against 480/270-kDa AnkG isoforms and Caspr. (**d**) Immunostaining of P22 spinal cords with antibodies against the peptide sequence encoded by *Ank3* exon 1e or 1b and βIV spectrin. Arrows point to paranodes. (**e**) P90 brain stems were labeled for AnkG (N106/36) and Caspr. (**f**) The schema shows the alternative first exons from different promoters and alternative splicing of exon 41 of *Ank3*. Scale bars = 5 μm (**c**), 3 μm (**d**), and 2.5 μm (**e**).